Aerospace Science and Technology 42 (2015) 415–428

Contents lists available at ScienceDirect

Aerospace Science and Technology

www.elsevier.com/locate/aescte

Artificial neural network based inverse design: Airfoils and wings

Gang Sun, Yanjie Sun, Shuyue Wang *

Dept. of Mechanics & Engineering Science, Fudan University, Shanghai 200433, Shanghai, PR China

ARTICLE INFO

Article history:
Received 20 October 2014
Received in revised form 30 December 2014
Accepted 6 January 2015
Available online 11 February 2015

Keywords:
Artificial neural network
Parameterization method
Wing
Airfoil
Inverse design

ABSTRACT

The numerical search for the optimum shape of airfoil/wing geometry is of great interest for aircraft and turbomachinery designers. However the conventional method of design and optimization, which is to repeat the process of modifying airfoil/wing geometry data based on the flow field calculation of initial geometry, is computationally intensive and time-costly. In lieu of this, this article introduces an applicable airfoil/wing inverse design method with the help of Artificial Neural Network and airfoil/wing database, so that a properly trained network should directly provide an airfoil/wing that fits the required aerodynamical features. Repeating the process itself being avoided, the design efficiency improves. This article will present the detail of setting up the airfoil/wing inverse design method and provide the verification of the applicability of the approach.

© 2015 Elsevier Masson SAS. All rights reserved.

1. Introduction

An advanced aerodynamic layout, which can reduce flight drag of a jet to increase its cruise efficiency and safety, is basically dependent on the design of an airplane's wings or more fundamentally, its airfoils. Wind tunnel was the major airfoil/wing designing tool. The first Boeing 747 took wind tunnel experiments for over 15,000 hours.[1] 1960s saw the introduction of CFD into the field that enhanced the development of airfoil/wing design [2]. The methods brought by CFD covered linear potential flow equation method, full velocity potential method with boundary layer correction, Euler equation method and Navier–Stokes equation method [12]. However before 1980s most design results involved quite much experience of designers, due to coupling variables in designs. It was hard then to set up a systematic design that was likely to reduce time and sources, because the conventional design requires the repeated process of *design–evaluation–improvement*. Compared with the wind-tunnel experiments, the conventional design methods performed better but still remain the necessary repetition of modifying during which designers' own experiment interferes. In addition, when the options of optimization method or optimizing direction were not selected properly, satisfactory results were hard to get. Therefore a new airfoil/wing design method of higher efficiency is what mechanics as a discipline as well as engineering application has been looking forward to.

Since 1990s, the rise of database technique and artificial intelligence technique has pushed the passenger jet aerodynamical design forward [1]. Aircraft manufacturers have access to their database that is made up of abundant designing experience and experiment data. The database gives proposal in prototype research and modification. Optimization methods including control theory optimization [11,17], Genetic Algorithm [24,26], Particle Swarm Optimization [25], and Artificial Neural Network [8,16] are carried out in the database. Compared with other machine learning methods which have been tried in shape optimization, ANN is able to provide more flexibility in building the calculating model without involving many parameters (e.g. chromosome in GA, or swarm picking in PSO, etc.) that have to be determined in specific cases. The inverse design case in this article could be regarded as one of the examples.

The technique of ANN raised the hopes for designers, for its swiftness and intelligence. There are precedents of ANN application in airfoil/wing design. Scholars make an ANN model of aerodynamical shape as a tool in geometrical analysis [10]. ANN has its reputation in making a nonlinear link between the inputs and outputs (in our case, a link from geometrical shape to its corresponding aerodynamical features, e.g. lift coefficients). The complexity of airfoil/wing shape design (multi-variables and small samples) does require a model that is intuitive, simple and not too specific; ANN can meet this request very well. As it turns out, design methods with ANN reduce calculation amount and time cost. Yet doubts remain on the reliability of the design result due to the unclear physical explanation of the ANN model. Many scholars have been working on that [5,23]. Bernstein introduced RANN (Replicative Artificial Neural Networks) [4] where inputs and outputs have the

* Corresponding author.
E-mail addresses: gang_sun@fudan.edu.cn (G. Sun), 11210290009@fudan.edu.cn (Y. Sun), sywang14@fudan.edu.cn (S. Wang).

[1] www.thic.org/pdf/Oct01/boeing.jgreen.011009.pdf.

http://dx.doi.org/10.1016/j.ast.2015.01.030
1270-9638/© 2015 Elsevier Masson SAS. All rights reserved.

same numbers of parameters, which is more than the number of neural nodes. Therefore, an effective data compression is available in analysis.

In recent years ANN has entered the inverse design of airfoils where ANN plays a role as a calculator based on a pre-set model. Kharal et al. [13] described the implementation of ANN for airfoil geometry determination. Instead of using full coordinates of the airfoil, Bezier–PARSEC (Parametric Airfoils and Wings, proposed by Sobieczky [20]) parameters were used to describe an airfoil. But Kharal's method has its shortcomings: its lack of full discretization due to the combination of Bezier and PARSEC, which still requires manual interference in parameterization, hindering the application and the optimization thereafter.

This article, in particular, introduces an inverse aerodynamic shape (i.e. airfoil or wing) design method that can directly inverse-design airfoils/wings whose geometry fits the expected/requested aerodynamic features (again, without repetitive process of conventional design–evaluation–improvement), based on an accumulated database of airfoils/wings and a properly trained Artificial Neural Network (time saved by which is of large magnitude, compared with conventional design method). To be specific, this article provides cases of an application of inverse design as a solution to the problem of the design of wings of a cruising passenger jet. In addition, by providing design results more efficiently and more accurately, the new airfoil/wing inverse design lays foundation for the optimization that may come later.

2. Establish the inverse design method of aerodynamic shape

2.1. Roadmap

Aerodynamic design in modern days has two major goals:

(i) Designers should take advantage of airfoil/wing database to accomplish a new approach in fast design.
(ii) The price of convenience should never be the loss of reliability.

Conventional aerodynamical design method Conventional aerodynamical design method, by definition, first gets the aerodynamic feature of a given airfoil under a certain flow condition by CFD or wind tunnel experiments, modifies the geometry of the airfoil according to aerodynamic knowledge and experience, and then repeats the above process until the outcome is satisfactory.

Inverse design method On the contrary, inverse design, by definition, can get the geometry of aerodynamic shape directly from the required aerodynamic features (usually input by designers).

In our case, ANN is used to set up the network linking aerodynamic features and geometry data, where SOM (Self-Organizing Map) network is used as a classifier to reduce the multi-variable problem's impact to the reliability of the ANN model (Fig. 1). Once the network is trained, the result can be obtained very quickly.

The steps to establish airfoil/wing inverse design approach are the following:

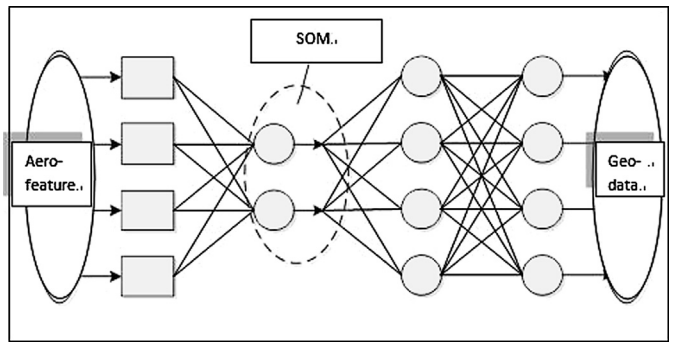

Fig. 1. An ANN model for inverse design.

Step 1 Extract essential geometry data from the parameterized aerodynamic shape. This is necessary for the application of ANN, which resembles the numerical code procedure in Genetic Algorithm.
Step 2 Obtain aerodynamic features from the results of the calculation/experiment of airfoil/wing in a flow condition.
Step 3 The database (its function: to give proposals to the ANN) is built.
Step 4 With SOM as a classifier to reduce the difficulty, ANN now sets up a model, which requires appropriate samples as the model's inputs and outputs.

2.2. Tools

2.2.1. Parameterization

The application of ANN's premise is parameterized database. Many parameterization methods have been used or discussed, e.g. orthogonal basis function method, Dick–Henne form function linear perturbation method [9], B spline method, PARSEC and CST (Class/Shape function Transformation) [14].

Samareh [18] evaluated 9 methods of parameterization with 10 principles. Sripawadkul [22] simplified the research by adding intuitiveness into 5 principles as criteria for parameterization method evaluation (shown in Table 1 with makers ranging from 0.0 to 4.0). The 5 principles:

Parsimony: as few variables as possible
Flawlessness: high uniformity of parameterized and original shapes
Orthogonality: no two aerodynamic shapes share the same set of parameters
Completeness: ensuring no strange/weird shape would appear
Intuitiveness: correlations between parameters and geometrical features

Padulo gave explanation to these five rules [15].

Table 1 tells us (despite the chance of generations of very few strange shapes which include situations where the upper surface crossed the lower surface in the middle of chord. This may be led by the less constraint given by PARSEC for the sake of high parsimony. Airfoils and wings with strange shapes can be detected by naked eyes and can be avoided by adjusting related parameters). PARSEC is generally better than other parameterization methods.

Table 1
Samareh's evaluation to parameterization [18].

Methods	Parsimony	Completeness	Orthogonality	Flawlessness	Intuitiveness
Ferguson's curve	4.0	2.4	0.0	4.0	2.0
Hicks–Henne	1.0	4.0	0.0	4.0	3.0
B-Spline	3.5	3.9	0.0	4.0	3.0
PARSEC	2.9	3.8	4.0	2.9	4.0
CST	2.9	3.7	4.0	4.0	4.0

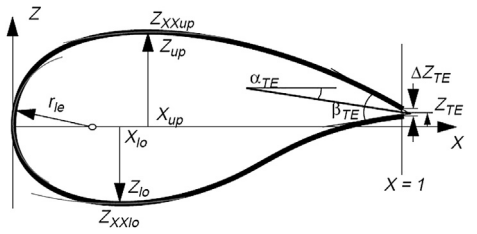

Fig. 2. PARSEC's geometry illustration [20].

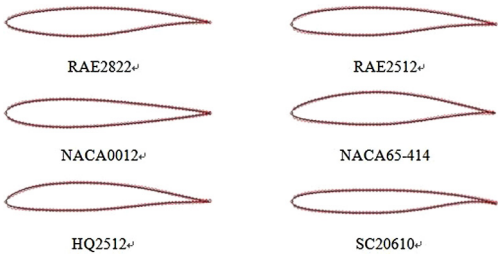

Fig. 3. PARSEC's reconstruction of 6 airfoils.

Therefore, this article selects PARSEC method to reconstruct airfoils and wings.

PARSEC PARSEC was developed by Sobieczky [20]. PARSEC is made up of 11 characteristic parameters that can describe an airfoil geometrically (Fig. 2). PARSEC has its advantages [7]:

- correlation between parameterization and aerodynamic parameters are bigger, for all the control points are given through the polynomials of the 11 PARSEC parameters;
- outline of the aerodynamic shape is smooth;
- the link between a parameter and a geometry feature is so tight that every value can be constrained easily thus eliminating errors of great magnitude.

PARSEC contains several parameters as follows: leading edge radius r_{le}, upper wing surface thickest position X_{up}, lower wing surface thickest position X_{lo}, upper wing surface maximum thickness Z_{up}, lower wing surface maximum thickness Z_{lo}, upper peak curvature Z_{xxup}, lower wing surface peak curvature Z_{xxlo}, tail width δZ_{TE}, tail vertical height Z_{TE}, tail wedge angle β_{TE}, tail direction angle α_{TE}, where tail wedge angle and direction angle are measured clockwise. Upper wing surface and lower wing surface curves can be obtained through polynomial fitting

$$z(x) = \sum_{n=1}^{6} a_n x^{n-1/2}$$

where a_n of upper and lower wing surface is provided by matrix equation as below [19].

$$\begin{bmatrix} 1 & 0 & 0 & 0 & 0 & 0 \\ x_{te}^{\frac{1}{2}} & x_{te}^{\frac{3}{2}} & x_{te}^{\frac{5}{2}} & x_{te}^{\frac{7}{2}} & x_{te}^{\frac{9}{2}} & x_{te}^{\frac{11}{2}} \\ x_{up}^{\frac{1}{2}} & x_{up}^{\frac{3}{2}} & x_{up}^{\frac{5}{2}} & x_{up}^{\frac{7}{2}} & x_{up}^{\frac{9}{2}} & x_{up}^{\frac{11}{2}} \\ \frac{1}{2}x_{te}^{\frac{-1}{2}} & \frac{3}{2}x_{te}^{\frac{1}{2}} & \frac{5}{2}x_{te}^{\frac{3}{2}} & \frac{7}{2}x_{te}^{\frac{5}{2}} & \frac{9}{2}x_{te}^{\frac{7}{2}} & \frac{11}{2}x_{te}^{\frac{9}{2}} \\ \frac{1}{2}x_{up}^{\frac{-1}{2}} & \frac{3}{2}x_{up}^{\frac{1}{2}} & \frac{5}{2}x_{up}^{\frac{3}{2}} & \frac{7}{2}x_{up}^{\frac{5}{2}} & \frac{9}{2}x_{up}^{\frac{7}{2}} & \frac{11}{2}x_{up}^{\frac{9}{2}} \\ \frac{-1}{4}x_{up}^{\frac{-3}{2}} & \frac{3}{4}x_{up}^{\frac{-1}{2}} & \frac{15}{4}x_{up}^{\frac{1}{2}} & \frac{35}{4}x_{up}^{\frac{3}{2}} & \frac{63}{4}x_{u}p^{\frac{5}{2}} & \frac{99}{4}x_{up}^{\frac{7}{2}} \end{bmatrix} \begin{bmatrix} a_1 \\ a_2 \\ a_3 \\ a_4 \\ a_5 \\ a_6 \end{bmatrix}$$

$$= \begin{bmatrix} \sqrt{2r_{le}} \\ z_{te} + \frac{\delta z_{te}}{2} \\ z_{up} \\ -\tan(\alpha_{te} + \beta_{te}) \\ 0 \\ z_{xx,up} \end{bmatrix}$$

Lower wing surface a_n's calculation is similar to that of upper wing surface, as follows:

$$\begin{bmatrix} 1 & 0 & 0 & 0 & 0 & 0 \\ x_{te}^{\frac{1}{2}} & x_{te}^{\frac{3}{2}} & x_{te}^{\frac{5}{2}} & x_{te}^{\frac{7}{2}} & x_{te}^{\frac{9}{2}} & x_{te}^{\frac{11}{2}} \\ x_{lo}^{\frac{1}{2}} & x_{lo}^{\frac{3}{2}} & x_{lo}^{\frac{5}{2}} & x_{lo}^{\frac{7}{2}} & x_{lo}^{\frac{9}{2}} & x_{lo}^{\frac{11}{2}} \\ \frac{1}{2}x_{te}^{\frac{-1}{2}} & \frac{3}{2}x_{te}^{\frac{1}{2}} & \frac{5}{2}x_{te}^{\frac{3}{2}} & \frac{7}{2}x_{te}^{\frac{5}{2}} & \frac{9}{2}x_{te}^{\frac{7}{2}} & \frac{11}{2}x_{te}^{\frac{9}{2}} \\ \frac{1}{2}x_{lo}^{\frac{-1}{2}} & \frac{3}{2}x_{lo}^{\frac{1}{2}} & \frac{5}{2}x_{lo}^{\frac{3}{2}} & \frac{7}{2}x_{lo}^{\frac{5}{2}} & \frac{9}{2}x_{lo}^{\frac{7}{2}} & \frac{11}{2}x_{lo}^{\frac{9}{2}} \\ \frac{-1}{4}x_{lo}^{\frac{-3}{2}} & \frac{3}{4}x_{lo}^{\frac{-1}{2}} & \frac{15}{4}x_{lo}^{\frac{1}{2}} & \frac{35}{4}x_{lo}^{\frac{3}{2}} & \frac{63}{4}x_{lo}^{\frac{5}{2}} & \frac{99}{4}x_{lo}^{\frac{7}{2}} \end{bmatrix} \begin{bmatrix} a_1 \\ a_2 \\ a_3 \\ a_4 \\ a_5 \\ a_6 \end{bmatrix}$$

$$= \begin{bmatrix} \sqrt{2r_{le}} \\ z_{te} - \frac{\delta z_{te}}{2} \\ z_{lo} \\ -\tan(\alpha_{te} - \beta_{te}) \\ 0 \\ z_{xx,lo} \end{bmatrix}$$

In order to verify PARSEC by comparing the results of PARSEC reconstruction from parameter extraction of airfoils and shapes of airfoils, we reconstruct with PARSEC the airfoils of RAE2822, RAE2512, NACA0012, NACA65-414, HQ2512, and SC20610, shown in Fig. 3. The verification is successful.

2.2.2. Flow field calculation

The information of aerodynamic features of airfoils and wings comes from flow field calculation in this article. This article uses full potential equations, boundary layer modification method and N–S equation method. The calculation of wing root flow field is done by FDNN program, which was designed and used by Department of Mechanics and Engineering Science of Fudan University in flow field calculation. The shape of frontal wing tip is calculated through N–S equation method.

Flow field calculation: airfoil BGKJ (Bauer–Garabedian–Korn–Jameson) [3] as an equation can be used to calculate flow field velocity potentials through transonic full velocity potentials equations with weak viscous interaction to account for strong viscous interaction [6], and gets the details of boundary layer through turbulence integration method. Fig. 4(a) shows the shape of classical RAE2822 airfoil which was selected as a validation case by the 16 partners of the EUROVAL (European Initiative on Validation of CFD Codes) European project. The result of BGKJ equation calculation and real pressure distribution are compared in Fig. 4(b).

Fig. 4(b) compares the pressure distribution of BGKJ equation calculation and experimental values, where the lower surface of airfoil fits pretty well and upper surface with slight deviation. Pressure distribution ahead of the shock wave fits well, while pressure distribution from the shock wave to the tail of airfoil sees deviation to some extent. BGKJ equation has great advantage over N–S equations with respect of time cost, especially in preliminary stages. This article uses BGKJ equations to do the flow-field calculation.

Flow field calculation: wing The calculation of wing–body combination is done with FDNN program. Considering the transonic flow

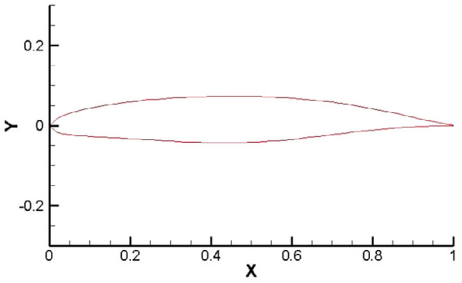

(a) The outline of RAE2822

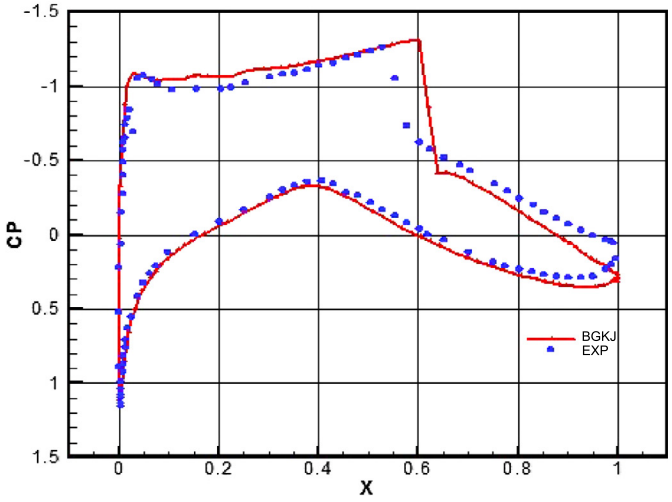

(b) Comparison of pressure distribution along the shape of airfoil RAE2822 between calculated result by BGKJ equation and experimental results[26]. Calculation conditions: Ma=0.75, Attack angle Alpha=2.72, Re=6,200,000.

Fig. 4. Flow field calculation on airfoil RAE2822.

over the wing and the wing–body-combination viscous separation area, main calculation method is set up on the viscous/inviscid coupling method within the boundary layer, where the inviscid outflow design calculation is based on approximate conservative full velocity potential method. On the wing–body-combination, a grid is generated through algebraic method, and the 3d compressible boundary layer over the wing is calculated through finite difference methods. The calculation method applied to viscous flow is Green integration.

Transonic flow calculation requires non-linear equations to deal with complexity. N–S equation can precisely predict the features of the flow field but at a fairly high price of time and computing resources. N–S is equivalent to Euler equation if the flow is considered inviscid. For complex shape of an airplane, Euler equation method still requires large amount of computing space. Assuming a very weak shock wave is in an inviscid flow field, the flow can be treated as isentropic. The magnitude of vortex is with higher order quantity so it can be ignored. Under the presumption of irrotationality full velocity potential method can be introduced to simplify Euler equation. The efficiency of 3d velocity potential equation program can be verified by calculating the flow filed of modern jet wing through FDNN (cf. Fig. 5).

Generally speaking, flow field calculation of velocity potential equation has its own merit as well as that of N–S equation does. For the sake of efficiency, design prefers velocity potentials; for the sake of accuracy, design prefers N–S equations method.

2.2.3. *Artificial neural network in this case*

Artificial Neural Network (ANN, for short) is computational model of machine learning as well as pattern recognition, which is inspired by an animal brains' central nervous systems. Its system of interconnected neurons can compute values from inputs and produce outputs as if experiencing a thinking period. Sets of adaptive weights (i.e. numerical parameters that are tuned by a learning algorithm) are given to neurons. The adaptive weights are activated during 'thinking period', i.e. training and prediction. Fig. 6(a) shows the basic model of artificial neuron, where $x_1, \ldots, x_n$ are the inputting signals with a weight coefficient w_{ij}, θ_j the threshold, f transferring function, o_j the outputting signal:

$$o_j = f\Big(\sum_{i=1}^{n} w_{ij}x_i - \theta_j\Big)$$

When the inputting signal hits the threshold, the neuron is activated so that outputting signal is sent out. The path that signals take varies in mainly two forms: hierarchical structure (e.g. BP (Back Propagation), RBF (Radial Basis Function) and GRNN (General Regression Neural Network)), and interconnected structure.

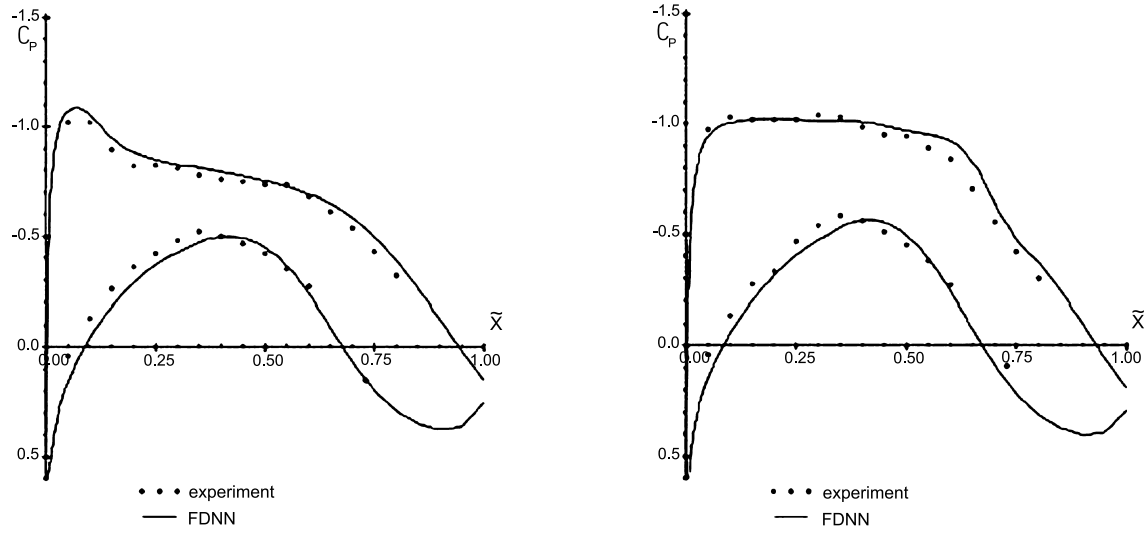

Fig. 5. The comparison of pressure distribution along the shape of a jet wing between calculated result by FDNN and experimental results. The calculation conditions: for the left image, $Ma = 0.71$, attack angle $Alpha = 2.72$, $Re = 6{,}200{,}000$.

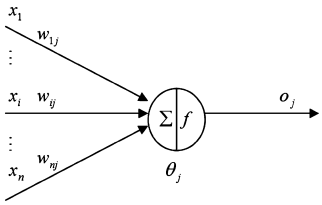

(a) The basic structure of ANN

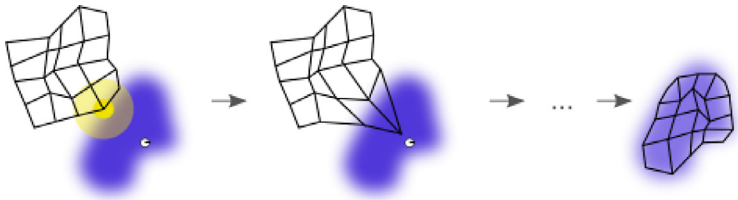

(b) An illustration of the training of a self-organizing map. The blue blob is the distribution of the training data, and the small white disc is the current training datum drawn from that distribution. At first (left) the SOM nodes are arbitrarily positioned in the data space. The node (highlighted in yellow) which is nearest to the training datum is selected. It is moved towards the training datum, as (to a lesser extent) are its neighbors on the grid. After many iterations the grid tends to approximate the data distribution (right).

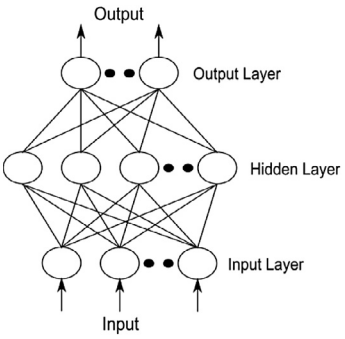

(c) Basic structure of a BP network

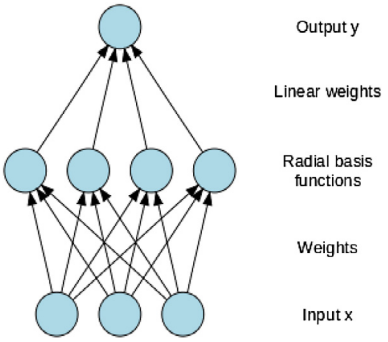

(d) Basic structure of a RBF network

Fig. 6. Some mainstream ANN algorithms.

A negative weight depresses the input and a positive weight enhances it.[2]

SOM A Self-Organizing Map (SOM) or Self-Organizing Feature Map (SOFM) is a type of ANN that is trained using unsupervised learning to produce a low-dimensional (typically two-dimensional), discretized representation of the input space of the training samples, called a map. Self-organizing maps are different from other artificial neural networks in the sense that they use a neighborhood function to preserve the topological properties of the input space.

SOM training classifies the neurons and their inputting paradigm. When inputting a signal, the neuron that is most similar to the signal responds thus a classification is finished (cf. Fig. 6(b)).

BP Back Propagation, an abbreviation for "backward propagation of errors", is a common method of training ANN used in conjunction with an optimization method such as gradient descent. The method calculates the gradient of a loss function with respect to all the weights in the network. The gradient is fed to the optimization method which in turn uses it to update the weights, in an attempt to minimize the loss function. Back propagation requires a known, desired output for each input value in order to calculate the loss function gradient. It is therefore usually considered to be a supervised learning method, although it is also used in some unsupervised networks such as autoencoders. It is a generalization of the delta rule to multi-layered feedforward networks, made possible by using the chain rule to iteratively compute gradients for each layer. Back propagation requires that the activation function used by the artificial neurons (or *nodes*) be differentiable (cf. Fig. 6(c)).

RBF and GRNN In the field of mathematical modeling, a radial basis function network (Fig. 6(d)) is an ANN that uses radial basis functions as activation functions. The output of the network is a linear combination of radial basis functions of the inputs and neuron parameters. Radial basis function networks have many uses, including function approximation, time series prediction, classification, and system control.

Generalized Regression Neural Network (GRNN) was proposed by Specht [21] as one of the variations of RBF. GRNN is strong at non-linear calculation problems.

3. Airfoil inverse design

This article hopes to find under certain working condition the correlation between airfoil/wing shape and its corresponding aerodynamic features, so that the expectation that a geometry can be obtained immediately by given request of aerodynamic features, can be realized.

[2] Thanks to http://en.wikipedia.org/wiki/Artificial_neural_network.

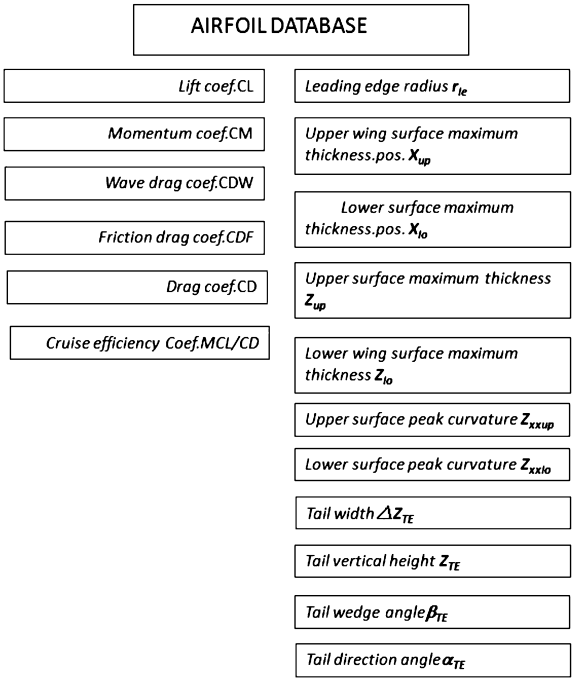

(a) What the airfoil database is made up of

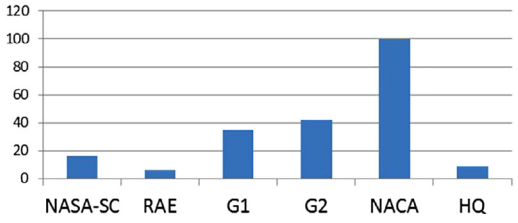

(b) The sources of the data of airfoil database

Parameters	Minimum Value	Maximum Value
CL	0.429	1.613
CM	-0.2526	0.003
CDW	-0.0002	0.04701
CDF	0.00342	0.0476
CD	0.00517	0.05522
MCL/CD	17.78	94.16
r_{le}	0.0034	0.0306
X_{up}	0.2927	0.5074
X_{lo}	0.275	0.4577
Z_{up}	0.0301	0.1116
Z_{lo}	0.0186	0.0923
$Zxxup$	0.02	1.1086
Z_{xxlo}	0.096	0.919
ΔZ_{TE}	0	0.0163
Z_{TE}	-0.0419	0.0082
b_{TE}	0.01	8.4622
a_{TE}	2.1599	16.6992

(c) The condition of the airfoils in the database

Fig. 7. The airfoil database.

3.1. Airfoil design request

Take RAE2822 as an example, according to simple sweptback theory in aerodynamics:

- $Ma_{2d} = Ma_{3d} \times \cos \chi_{1/4}$,
- $cl_{2d} = F \times CL_{3d} / \cos^2 \chi_{1/4}$, $F = 1.1, 1.2$,

where Ma_{3d} is the speed at which the wing–body flies, Ma_{2d} is the speed that is the tangential component to the airfoil on the wing due to the effect of swept angle, and $\chi_{1/4}$ is the swept angle of quarter chord. In our case, $\chi_{1/4} = 25$ deg. According to the design request for supercritical wing, the cruise Mach is 0.78. In the same way, CL_{3d} is the drag force coefficient of the wing–body and CL_{2d} is the component of CL_{3d} that is tangential to airfoil. Therefore, the condition in this case is:

Table 2
The 4 randomly picked airfoils' condition, where Cl is the lift coefficient, CD the drag coefficient, and MCL/CD the cruise efficiency.

Airfoil No.	CL	CD	MCL/CD
1	0.7922	0.0109	51.80
2	0.6911	0.0070	69.82
3	0.8113	0.0101	56.94
4	0.7329	0.0076	68.33

- $Ma_{2d} = 0.705$,
- attack angle $\alpha = 2.53$ deg,
- $Re = 23{,}000{,}000$.

3.2. Airfoil database establishment

11 shape parameters are obtained by PARSEC parameterization (cf. Fig. 7(a)). The aerodynamical features of the airfoils are also

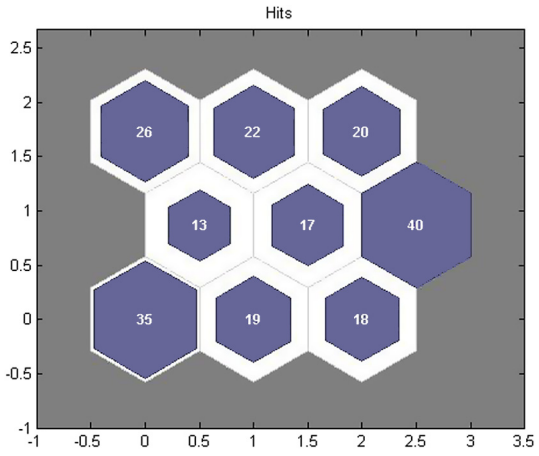

Fig. 8. The outcome of SOM classification to the airfoil database: 9 classes, 200 training steps.

obtained by flow field calculation. Therefore for an airfoil its aerodynamic features are matched with its shape parameters through ANN. The airfoil database contains 208 airfoils, which is a small number considering numbers of dimensions involved in the question. Fig. 7(b) shows the source and proportion of airfoils. An airfoil database needs high efficiency and completeness, so every airfoil should be fairly good in aerodynamic performance and the range the airfoils' geometry covers should be wide enough, which is shown in Fig. 6(c). The existence to the solution could be proved if the target aerodynamical requests locate within the range of the database, if an abstract multi-hypersurface is considered. Under this assumption, the data in the database and the data that is produced through ANN-aided inverse design system all lie in that hypersurface. Therefore the inverse problem can be, in a way, seen as a data fitting problem.

3.3. Conflict between multi-dimensionality and small sample: classification

A given geometrical shape of airfoil provides a certain and unique aerodynamical feature data under given flow condition. The aerodynamic feature is function of geometrical shape but not vice versa. There may be more than one set of geometrical shape that fits the aerodynamic feature given by designers, especially when the target aerodynamical feature is not multi-objective (e.g. in a case where our only concern is lift–drag ratio).

Classification, which is done through SOM training (Fig. 1), can be a good solution to the conflict between problem's multi-dimensionality and its small-sampleness without too much interference to details in ANN's intelligent inverse deign. Based upon the high fidelity of PARSEC as a parameterization method, presume that every parameter is independent to each other, and the problem has dimensions of 11 at least (which is very difficult in mathematics). The solution to this (Fig. 8) can alleviate the multi-dimensionless of the problem with high similarities.

3.4. Artificial Neural Network in airfoil inverse design: comparison

Mainstream ANN algorithms are BP, RBF and GRNN. Hereafter this article will discuss which network should be applied to airfoil inverse design. Comparisons of the three networks in experiment will lead to conclusion.

BP configuration: **learning algorithm** *Learngdm*
input neuron transferring function tan *sig*
output neuron transferring function *purelin*
error range of network training 10^{-5}
training step *0.1*
top limit of steps *1000*
hidden layers *7*

RBF configuration: **hidden layer activation function** *Gaussian nucleus function*
radius base function expansion speed *0.8*
hidden layer nodes *as many as input layer nodes numbers*

GRNN configuration: **expansion const** *0.1 0.2, in order to seek accurate solution*
interval *0.1*

Data normalization comes before data training. Four airfoils' data are randomly taken out (Table 2).

Error analysis of different ANN outcomes' aerodynamical features Airfoil inverse design models are established respectively through BP, RBF and GRNN. Definition of relative error is as follows:

$$\sigma = \frac{Y_i - Y_i'}{Y_i'}$$

where Y_i' is initial values and Y_i is anticipated value.

Table 3
Different ANNs are applied to the 4 previously taken airfoils.

Nos.-ann	CL	σ_{CL}%	CD	σ_{CD}%	MCL/CD	$\sigma_{MCL/CD}$%
1-BP	0.7791	−1.65	0.0106	−2.75	52.17	0.71
2-BP	0.7038	1.84	0.0069	−1.43	72.28	3.52
3-BP	0.7993	−1.48	0.0105	3.96	54.18	−4.85
4-BP	0.7057	−3.71	0.0076	0	66.03	−3.37
$\lvert\bar{\sigma}\rvert$		2.17		2.04		3.11
1-RBF	0.7900	−0.28	0.0132	21.10	42.57	−17.82
2-RBF	0.7221	4.49	0.0085	21.43	60.50	−13.35
3-RBF	0.8301	2.32	0.0116	14.85	50.77	−10.84
4-RBF	0.7514	2.52	0.0068	−10.53	79.03	15.66
$\lvert\bar{\sigma}\rvert$		2.40		16.98		14.42
1-GRNN	0.7848	−0.93	0.0096	−11.93	58.02	12.01
2-GRNN	0.7473	8.13	0.0080	14.29	66.48	−4.78
3-GRNN	0.8066	−0.58	0.0089	−11.88	64.27	13.66
4-GRNN	0.8578	17.04	0.0093	22.37	65.24	−4.52
$\lvert\bar{\sigma}\rvert$		6.67		15.12		8.74

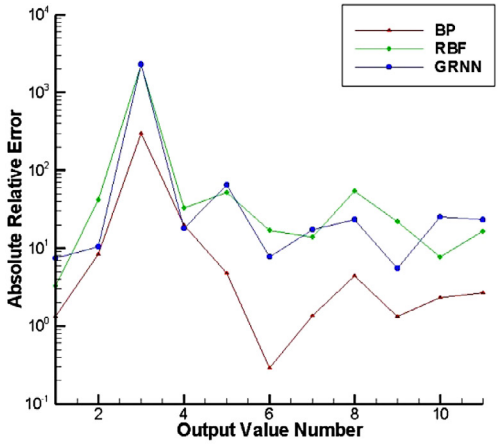

(a) The 1st airfoil error analysis between different ANNs

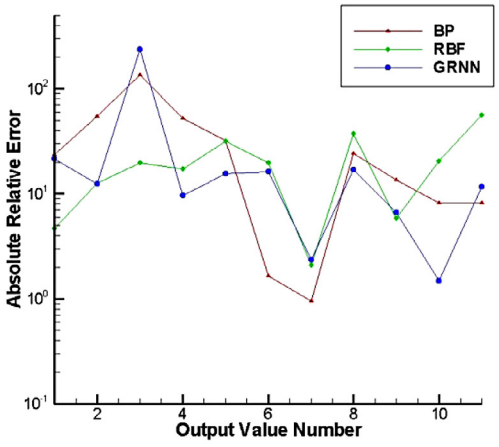

(b) The 2nd airfoil error analysis between different ANNs

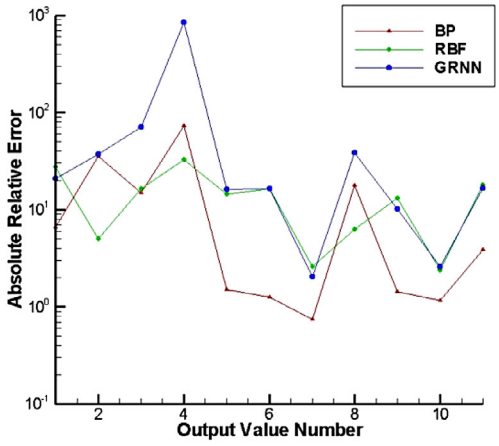

(c) The 3rd airfoil error analysis between different ANNs

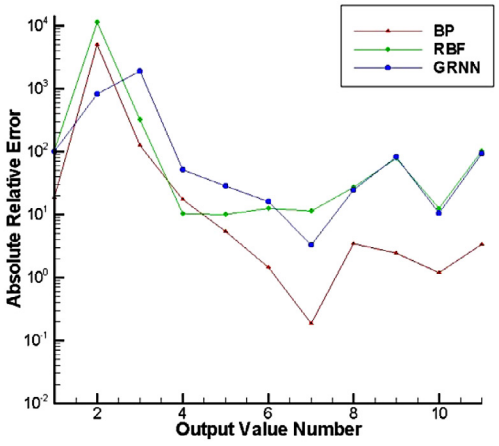

(d) The 4th airfoil error analysis between different ANNs

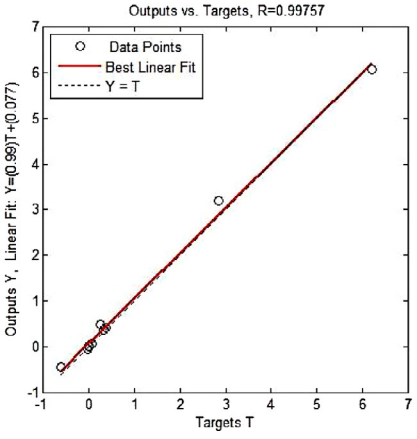

(e) The BP regression analysis of samples

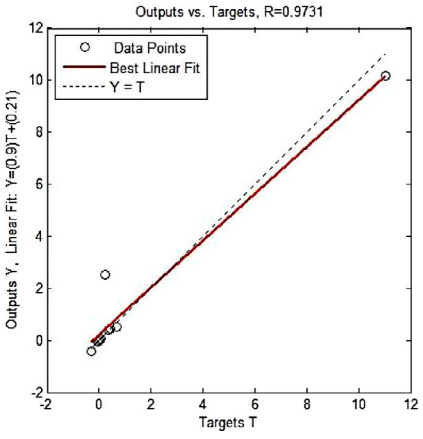

(f) The RBF regression analysis of samples

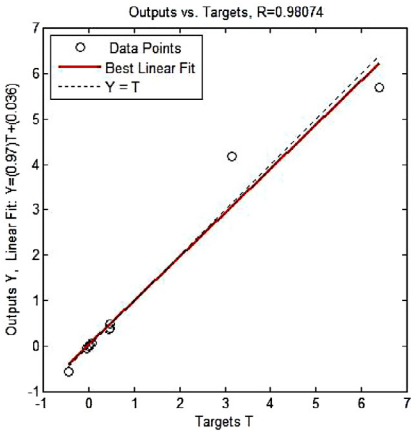

(g) The GRNN regression analysis of samples

Fig. 9. Error and regression analysis of three ANN algorithms applied on the 4 picked airfoils. (For interpretation of the references to color in this figure legend, the reader is referred to the web version of this article.)

Different ANNs are applied to the 4 previously taken airfoils, the results of which are in Table 3.

Error and regression analysis of the results that come from different ANNs Fig. 9(a), Fig. 9(b), Fig. 9(c), and Fig. 9(d) show the contrasts between real outputs and anticipated outputs of 11 geometrical parameters of each experiment. The abscissa is the number of geometrical parameters and ordinates are the relative error of geometrical parameter. correspondingly. Red, green and blue lines stand respectively for BP, RBF and GRNN.

Relative error speaking, BP network performs better than RBF and GRNN. An analysis of the rate of change between real and expected output is conducted with the help of postreg function and linear regression. Fig. 9(e), Fig. 9(f), and Fig. 9(g) show the result where Y is expected output and T is the real output. The correlation coefficient R of BP is 0.99757, for RBF, 0.9731; GRNN, 0.98074.

Table 4
Airfoil design request, with $Ma_{2d} = 0.705$, $Re =$ 23,000,000, angle of attack 2.53 deg.

Lift coef.[a]	0.8
Momentum coef.	−0.09
Wave drag coef.	0.0008
Friction coef.	0.006
Drag coef.[a]	0.06
Cruise efficiency[a]	90

[a] Main aerodynamical parameters.

Table 5
Inverse design result.

r_{le}	0.00876
X_{up}	0.4598
X_{lo}	0.4319
Z_{up}	0.07322
Z_{lo}	−0.04333
Z_{xxup}	−0.4231
Z_{xxlo}	0.6011
ΔZ_{TE}	0.0013
Z_{TE}	−0.0003
β_{TE}	4.7754
α_{TE}	5.0864

Table 6
Aerodynamical features of output of airfoil inverse design and those of real airfoil.

	Inverse designed	Actual	Relative error
CL	0.8049	0.8	0.61
MCL/CD	90.53	90	0.59

Considering generalization capability and relative error, this article selects BP as algorithm of airfoil inverse design model establishing.

3.5. Case: airfoil inverse design based on BP

Task of airfoil inverse design: design an airfoil that fits the aerodynamical request, as is shown in Table 4. The three parameters are given by designer directly and the rest are given through interpolation. The outcome of airfoil inverse design is shown in Table 5 and the shape of the product can be seen in Fig. 10.

Flow field calculation is done as a verification of airfoil inverse design. Table 6 shows the contrast of aerodynamical features of output of airfoil inverse design and those of real airfoil. All aerodynamical parameters locate in an acceptable range of error.

4. Wing inverse design: extension from airfoil inverse design

4.1. Wing database

Compared with an airfoil, a wing is complex in geometrical description. Fig. 11 shows the wing–body combination. Each wing has 6 airfoils which locate at 0, 0.2, 0.4, 0.6, 0.8 of the distance from wing root to wing tip. Airfoils in a wing are selected from airfoil database that is previously set up.

In addition to airfoil parameters, a wing needs another two parameters that are relative thickness and twisting angle. Totally, constraints on a wing have $6 \times 11 + 12 = 78$ parameters. Now, the 78-parameter wings comprise the wing database, as well as their corresponding aerodynamical features that have been calculated/experimented (Fig. 12).

Fig. 13 shows that the numbers of dimensions of input and output in wing inverse design are different, which is not the case in airfoil inverse design. The task of wing inverse design ANN model is to establish non-linear matches between inputs and outputs through automated learning.

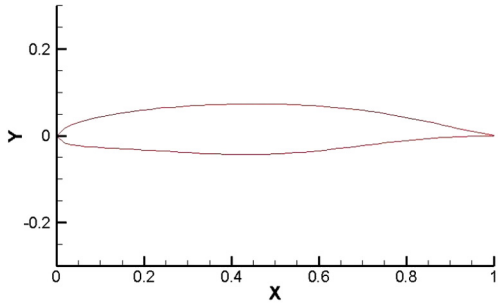

Fig. 10. The shape of the airfoil inverse design product.

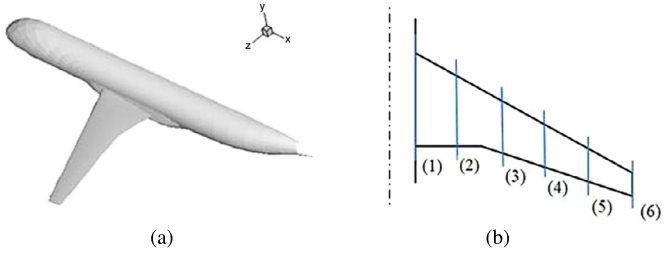

Fig. 11. Illustration of wing–body combination and wing structures.

The aerodynamical features represented by parameters have the values shown in Table 7, where MCL/CD is $Ma_{3d} * CL/CD$, a coefficient to measure cruise efficiency of wing–fuselage combination, CL is lift coefficient of wing–fuselage combination, CD the drag coefficient, CDP the part of wing–fuselage combination drag coefficient that is led by pressure difference, CDI the part of wing–fuselage combination drag coefficient that is led by induced flow under the wing, CDW the part of wing–fuselage combination drag coefficient that is led by shock waves, CLWING the wing's contribution to the wing–fuselage combination lift coefficient, CDWING the wing's contribution to the wing–fuselage combination drag coefficient, CMWING the wing's contribution to the wing–fuselage combination torque coefficient.

4.2. SOM classification in wing database

The SOM classification in wing database is shown in Fig. 14.

4.3. Artificial neural network in wing inverse design: comparison

BP with 20 hidden layer nodes has a structure of 9-20-78. The configuration of three ANN is the same as that in airfoil experiments. Select randomly 4 groups of wings from wing database. Their aerodynamical features are shown in Table 8.

Table 9 is the error analysis of outcomes of ANNs that have been applied to 4 randomly picked wings:

From the above analysis of predicted lift coefficients and cruise efficiency factors, we know the predicted error locates in the range of 3% and GRNN's in the range of 0.4%. Therefore we come to a conclusion that GRNN may perform better in wing inverse design. The analysis between different ANN of the 4 picked wings is shown in Fig. 15.

Regression analysis Fig. 15(e), Fig. 15(f), and Fig. 15(g) show that for the 4 picked wings the correlation coefficient R of BP is 0.98246, for RBF, 0.93577; GRNN, close to 1.

There might be two reasons as explanation to the different outcome of different ANN algorithms applied to the problem.

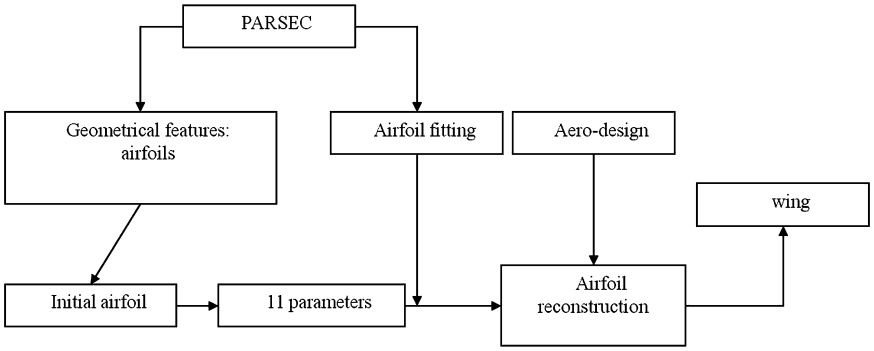

Fig. 12. Wing reconstruction flow chart.

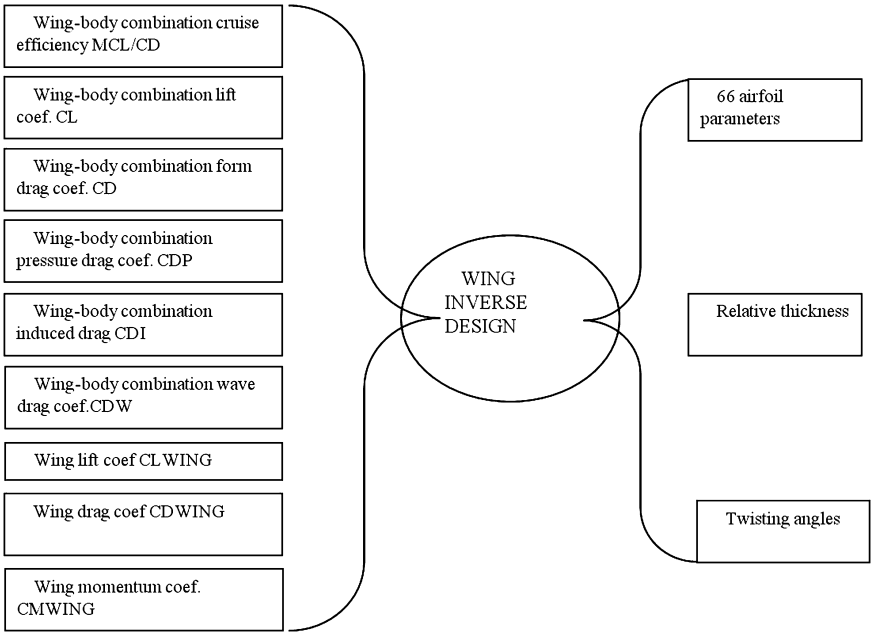

Fig. 13. Wing inverse design's inputs and outputs under ANN.

Table 7
The condition of wings in the database.

Parameters	Minimum value	Maximum value
MCL/CD	24.00764	26.96900
CL	0.4081	0.5962
CD	0.00751	0.01513
CDP	0.00633	0.01230
CDI	0.00003	0.00077
CDW	0.1817	0.27524
CLWING	0.34854	0.51882
CDWING	0.00668	0.01317
CMWING	−0.17852	0.12929
Relative thickness	0.7641	1.09878
Twisting angle/°	−0.304	3.23

1. The configuration of BP algorithm plays important role in the result, because there are many parameters in BP function while GRNN is less complex in that matter.
2. As is said the number of dimensions of output in wing inverse design is bigger than its counterpart in airfoil inverse design, which leads to slow down the BP calculating speed, while leaves no impact to GRNN and RBF.

Therefore it is worth mentioning that comparison of ANN algorithm performance should be treated as a variation of a set of parameters.

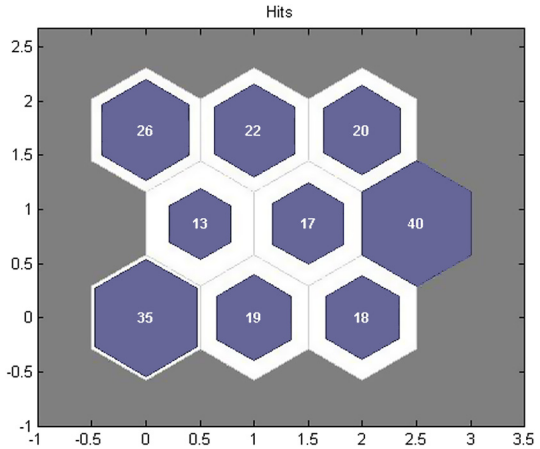

Fig. 14. The SOM classification in wing database.

Table 8
The 4 randomly picked wings' condition.

No.	MCL/CD	CL	CLWING
1	25.5519	0.4907	0.4219
2	25.5109	0.4616	0.3962
3	25.1194	0.5101	0.4394
4	25.7994	0.5023	0.4335

Table 9
Different ANNs are applied to the 4 randomly taken wings.

Nos. and ANN	MCL/CD	$\sigma_{MCL/CD}\%$	CL	$\sigma_{CL}\%$	CLWING	$\sigma_{CLWING}\%$
1-BP	24.7479	−3.15	0.5055	3.02	0.4373	3.65
2-BP	25.7005	0.74	0.4515	−2.19	0.3904	−1.46
3-BP	25.0491	−0.28	0.5284	3.59	0.4593	4.53
4-BP	25.6568	−0.55	0.5123	1.99	0.4460	2.88
$\lvert\bar{\sigma}\rvert$		1.18		2.70		3.13
1-RBF	25.5357	−0.06	0.4921	0.29	0.4261	1.00
2-RBF	25.7697	1.01	0.4746	2.82	0.4099	3.46
3-RBF	25.1465	0.11	0.4911	−3.72	0.4244	−3.41
4-RBF	25.0046	−3.08	0.5198	3.48	0.4494	3.67
$\lvert\bar{\sigma}\rvert$		1.070		2.58		2.89
1-GRNN	25.5573	0.02	0.4935	0.57	0.4275	1.33
2-GRNN	25.5406	0.12	0.4729	2.45	0.4089	3.21
3-GRNN	25.0596	−0.24	0.5212	2.18	0.4523	2.94
4-GRNN	25.8287	0.11	0.4983	−0.80	0.4316	−0.44
$\lvert\bar{\sigma}\rvert$		0.12		1.50		1.98

4.4. Case: wing inverse design base on GRNN

In this sample we will deal with a task to design a supercritical wing that satisfies: Its wing–body combination lift/drag ratio 25.8, lift coefficient 0.5, form drag coefficient 0.0105, induced drag coefficient 0.009, wave drag coefficient 0.00017, momentum coefficient 0.23, wing lift coefficient 0.43, wing drag coefficient 0.0095, and wing momentum coefficient −0.13, under:

- $Ma = 0.78$,
- $\alpha = 2.53$ deg,
- $Re = 23{,}000{,}000$.

Main characteristics of aerodynamic features (e.g. wing lift/drag ratio) are given by designer, while the rest of the parameters are obtained through interpolation based on database.

Classified with SOM with respect to aerodynamic features, the wing inverse design model takes one set of aerodynamic feature from the database as input and gives a set of geometrical data as outcome through GRNN. The result is also tested for verification.

With wing inverse design method, 78 wing shape parameters of a wing are obtained based on given aerodynamic feature. Fig. 16(a), Fig. 16(b), Fig. 16(c), and Fig. 16(d) describe the details of the generated wing.

As a step of verification, we calculate the generated wing's aerodynamic features, the result of which will be compared with the initial aerodynamical feature data (real wing's data) in Table 10.

The accuracy of wing inverse design is largely dependent on the width and depth of database. The depth, by definition, is the range that data locate in the depth, by definition is the good distribution of data with respect of target aerodynamic features. Adequate amount of data of certain type should be supplied to wing inverse design database.

In order to further eliminate error of wing inverse design product, the option of expanding database is always open.

5. Conclusion

The inverse design of airfoils/wings helps designers take the expected airfoil/wing DIRECTLY according to given aerodynamical requests, rather than cut-and-trying in other optimizational methods. This will definitely accelerate the designing process. The top concern of airfoil/wing inverse design:

1. This article compares some kinds of parameterization method. For the sake of accuracy orthogonality and intuitiveness, we selected PARSEC as the parameterization method.
2. An inverse design of aerodynamic shape has been set up based on database as well as a series of aerodynamic features e.g. lift/drag coefficient, momentum coefficient, and cruise efficiency factor, etc. through ANN model.
3. Airfoil inverse design is built on an airfoil database of 208 airfoils. After evaluating the performance of three ANN algorithms we selected BP as the algorithm in airfoil inverse design. Verification experiment tells us the relative error of lift coefficients and cruise efficiency is with the range of 0.61% and 0.59%, respectively.
4. Similar to airfoil inverse design, the wing airfoil design is built on an airfoil database of 210 airfoils. After evaluating the performance of three ANN algorithms we selected BP as the algorithm in wing inverse design. Verification experiment tells us the relative error of cruise efficiency, wing–body combination lift coefficient, and wing lift coefficient are with the range of 0.39% and 2.22%, and 1.33%, respectively.

On the whole, this article has accomplished the following works:

1. Discussing the parameterization methods based on accuracy and orthogonality and practice in aerodynamic shape design; this article uses PARSEC as the parameterization method, thus establishing a database that consists of airfoil/wing's geometry and their aerodynamic features e.g. lift, drag, efficiency of cruise etc.
2. Established the theory of airfoil/wing inverse design model with ANN.
3. Application of airfoil inverse design. With a database of 208 airfoil samples, this article compares BP, RBF and GRNN. This article decides to use BP as the ANN tool for airfoil inverse design. According to verification, the result error locates in an acceptable range, which echoes the research in [13].
4. Application of wing inverse design. With a database of 210 wing samples, this article decides to use GRNN as the ANN tool based on the consideration of error analysis and network generalization. The result of the established wing inverse design stands up to the verifications.

Conclusively the inverse design method developed by this article performs better than many conventional design methods in accuracy and efficiency. As a matter of fact the success of ANN application in inverse design shows a possibility of its use in optimization based on inverse design concept.

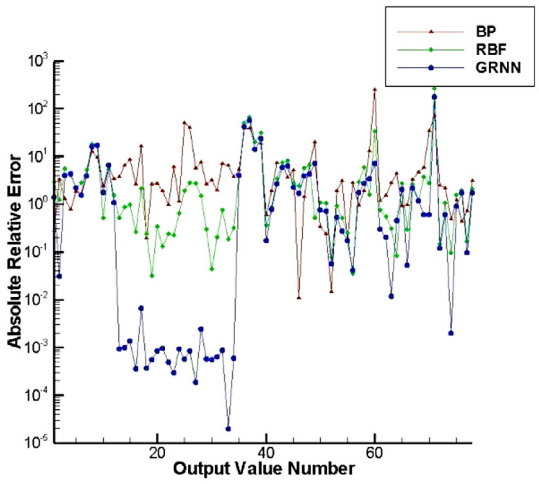

(a) The 1st wing error analysis between different ANNs

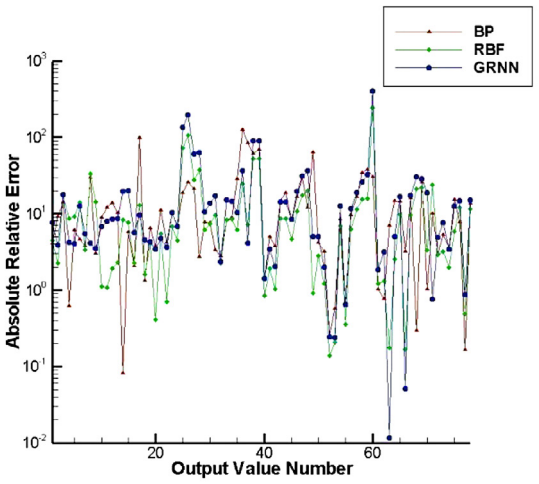

(b) The 2rd wing error analysis between different ANNs

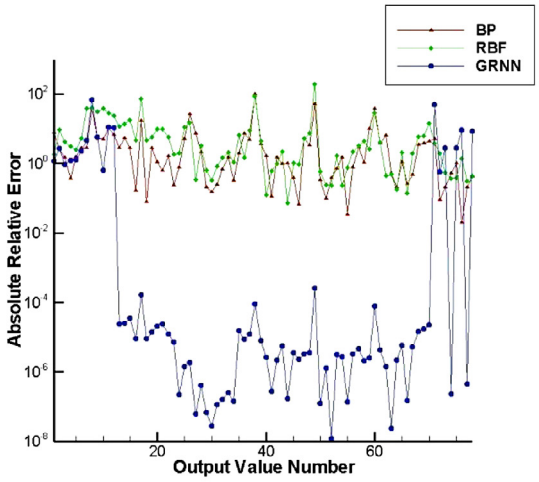

(c) The 2rd wing error analysis between different ANNs

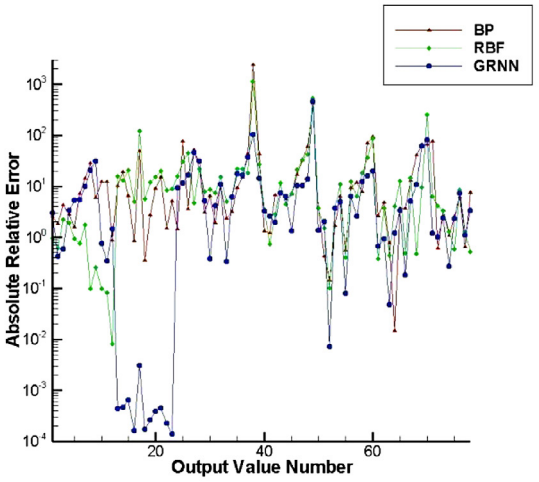

(d) The 4th wing error analysis between different ANNs

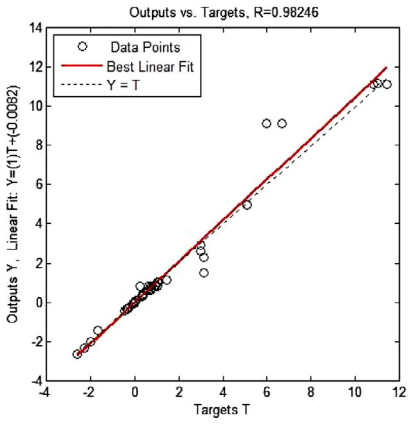

(e) BP regression analysis of the 4 wings

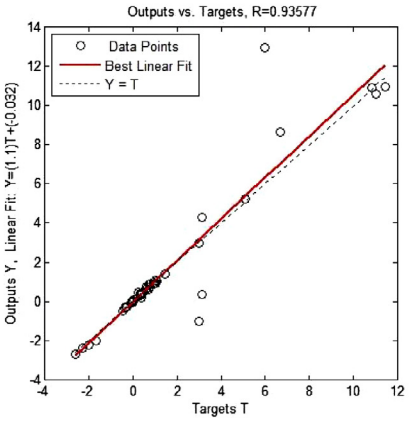

(f) RBF regression analysis of the 4 wings

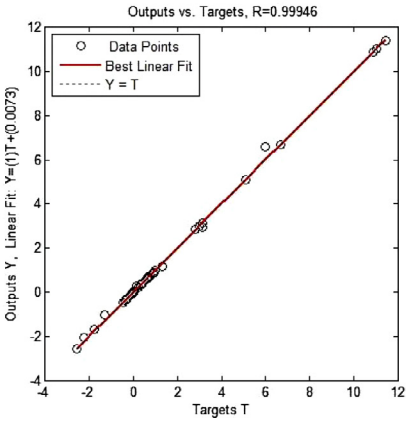

(g) GRNN regression analysis of the 4 wings

Fig. 15. Error analysis and correlation coefficients of the 4 picked wings.

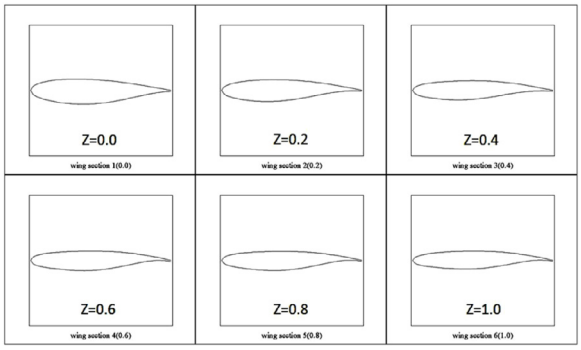

(a) Geometrical shapes along the axis of the generated wing

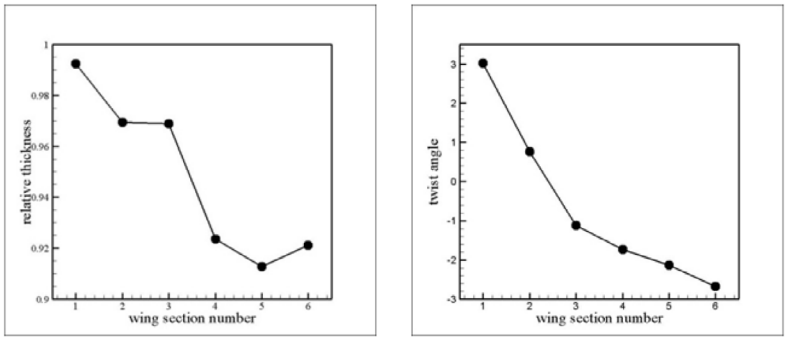

(b) Thickness distribution and twisting angles distribution along the axis of the generated wing

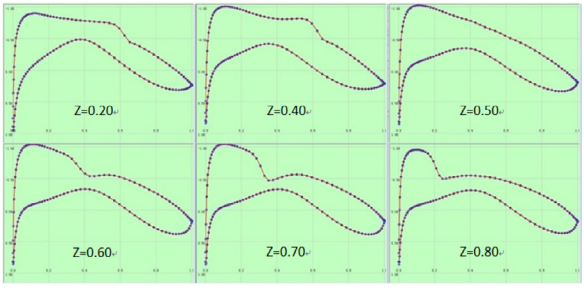

(c) Pressure distribution along the axis of the generated wing

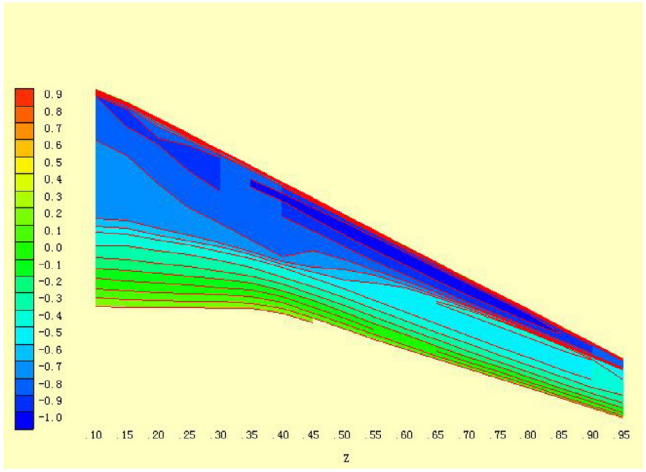

(d) Pressure distribution on the surface of the generated wing

Fig. 16. The condition of the generated wing.

Table 10
Comparison of the generated wing and the expected one.

Parameters	Generated	Expected	Relative error
MCL/CD	25.69939	25.8	−0.39
CL	0.4889	0.5	−2.22
CLWING	0.42428	0.43	−1.33

Conflict of interest statement

The authors declared that they have no conflicts of interest to this work.

Acknowledgement

This article has been funded by China 973 National Project (2014CB744800) “Study on the mechanism of drag reduction of large passenger aircraft: the mechanism of vorticity-led drag”.

References

[1] AIAA Multidisciplinary Design Optimization Technical Committee, Current state of the art on multidisciplinary design optimization (MDO), Tech. rep., AIAA, 1991.
[2] H. Ball, V. Lee, J. Mcleod, W. Moran, E. Wadsworth, Computerized aircraft synthesis, J. Aircr. 4 (5) (1967) 402–408.
[3] F. Bauer, P. Garabedian, D. Korn, A. Jameson, in: Lecture Notes in Economics and Mathematical Systems, vol. 176, 1975, 1970, Science 3.
[4] A.V. Bernstein, A.P. Kuleshov, Y.N. Sviridenko, V. Vyshinsky, Fast aerodynamic model for design technology, in: Proceedings of West–East High Speed Flow Field Conference, 2007, pp. 19–22.
[5] D. Ciresan, U. Meier, J. Schmidhuber, Multi-column deep neural networks for image classification, in: 2012 IEEE Conference on Computer Vision and Pattern Recognition (CVPR), IEEE, 2012, pp. 3642–3649.
[6] E.E. Covert, Thrust and Drag: Its Prediction and Verification, Progress in Astronautics and Aeronautics, vol. 98, AIAA, 1985.
[7] P. Della Vecchia, E. Daniele, An airfoil shape optimization technique coupling PARSEC parameterization and evolutionary algorithm, Aerosp. Sci. Technol. 32 (1) (2014) 103–110.
[8] X. Fan, T. Herbert, J. Haritonidis, Transition control with neural networks, AIAA 95-0674, in: 33rd AIAA Aerospace Sciences Meetings and Exhibit, AIAA, Reno, NV, 1995.
[9] R.M. Hicks, P.A. Henne, Wing design by numerical optimization, J. Aircr. 15 (7) (1978) 407–412.
[10] J. Huang, H. Su, X. Zhao, Airfoil aerodynamical coefficients prediction based on BP neural network, Aeronaut. Eng. Progress 1 (1) (2010) 36–39.
[11] A. Jameson, L. Martinelli, N. Pierce, Optimum aerodynamic design using the Navier–Stokes equations, Theor. Comput. Fluid Dyn. 10 (1–4) (1998) 213–237.
[12] F.T. Johnson, E.N. Tinoco, N.J. Yu, Thirty years of development and application of CFD at Boeing Commercial Airplanes, Seattle, Comput. Fluids 34 (10) (2005) 1115–1151.
[13] A. Kharal, A. Saleem, Neural networks based airfoil generation for a given Cp using Bezier–PARSEC parameterization, Aerosp. Sci. Technol. 23 (1) (2012) 330–344.
[14] B.M. Kulfan, J.E. Bussoletti, Fundamental parametric geometry representations for aircraft component shapes, in: 11th AIAA/ISSMO Multidisciplinary Analysis and Optimization Conference, 2006, pp. 1–42.
[15] M. Padulo, J. Maginot, M. Guenov, C. Holden, Airfoil design under uncertainty with robust geometric parameterization, in: 50th AIAA/ASME/ASCE/AHS/ASC Structure, Structural Dynamics, and Materials Conference, Palm Springs, CA, 2009, 2009-2270.
[16] M.M. Rai, Robust optimal aerodynamic design using evolutionary methods and neural networks, in: 42nd AIAA Aerospace Sciences Meetings and Exhibit, AIAA, Reno, NV, 2004.
[17] J. Reuther, A. Jameson, Aerodynamic shape optimization of wing and wing–body configurations using control theory, AIAA Paper 95-0123, 1995.

[18] J.A. Samareh, A survey of shape parameterization techniques, in: NASA Conference Publication, Citeseer, 1999, pp. 333–344.
[19] U. Selvakumar, P. Mukesh, Aerodynamic shape optimization using computer mapping of natural evolution process, in: 2010 2nd International Conference on Computer Engineering and Technology (ICCET), vol. 5, IEEE, 2010, pp. 367–371.
[20] H. Sobieczky, Parametric airfoils and wings, in: Recent Development of Aerodynamic Design Methodologies, Springer, 1999, pp. 71–87.
[21] D.F. Specht, A general regression neural network, IEEE Trans. Neural Netw. 2 (6) (1991) 568–576.
[22] V. Sripawadkul, M. Padulo, M. Guenov, A comparison of airfoil shape parameterization techniques for early design optimization, in: 13th AIAA/ISSMO Multidisciplinary Analysis Optimization Conference, 2010, 2010-9050.
[23] A. Verkhratsky, V. Parpura, J.J. Rodríguez, Where the thoughts dwell: the physiology of neuronal–glial "diffuse neural net", Brains Res. Rev. 66 (1) (2011) 133–151.
[24] W. Xiao-peng, G. Zheng-hong, et al., Airfoil aerodynamical optimization based on Genetic Algorithm, Aerodyn. J. 18 (03) (2000) 324–329.
[25] P. Xu, C. Jiang, Airfoil optimization based on PSO algorithm, Airplane Des. 28 (5) (2008) 6–9.
[26] X. Xu, Z. Zhou, Advanced UAV airfoil aerodynamical design method research, Flight Mech. 27 (2) (2009) 24–27.